



On Tracking Aeroelastic Modes in Stability Analysis Using Left and Right Eigenvectors

Xiaochen Hang* and Qingguo Fei†

Southeast University, Nanjing, Jiangsu 211189, People's Republic of China

and

Weihua Su‡

The University of Alabama, Tuscaloosa, Alabama 35487-0280

DOI: 10.2514/1.J057297

Mode tracking is one of the critical problems in aeroelastic stability analysis. A novel mode tracking method is discussed in this paper using both left and right eigenvectors of aeroelastic systems. Orthogonality between left and right eigenvectors of aeroelastic systems is assessed, which helps to identify and track the aeroelastic modes versus airspeeds. The developed mode tracking method is then applied in aeroelastic stability analyses of various wing and aircraft configurations, modeled by using different aeroelastic formulations. In numerical studies, mode tracking results from the new method are compared with those of the traditional methods, such as the approach based on modal assurance criterion of right eigenvectors of aeroelastic systems. From the studies, the advantages of the new method introduced in this paper are highlighted. It is verified that the new approach is more effective and accurate in tracking aeroelastic modes, and it is also able to accommodate different aeroelastic formulations and problems.

Nomenclature

A	=	aeroelastic system matrix	M_A, C_A, K_A	=	aerodynamic inertia, damping, and stiffness matrices
A_i	=	coefficient matrix of the rational function approximation, $i = 0, 1, 2, \dots$	m	=	total mass of airfoil, kg/m
a	=	dimensionless location of elastic axis behind midchord of airfoil	N	=	number of inflow states or number of rational functions
b	=	semichord of airfoil, m	Q	=	aerodynamic influence coefficient matrix
\bar{b}	=	coefficients of inflow states	q	=	elastic degrees of freedom
C_1, C_2	=	coefficients in Wagner's function	R	=	aerodynamic load vector
\bar{c}, \bar{W}	=	coefficient matrices in inflow equation	S, \tilde{S}	=	matrices for checking orthogonality between left and right eigenvectors
D	=	coefficient matrix of λ	S_α	=	structural imbalance of airfoil, kg
E	=	coefficient matrix of λ in aerodynamic state equation	s	=	Laplace variable
F	=	coefficient matrix of \ddot{q} in aerodynamic state equation	T	=	matrix for checking orthogonality between right eigenvectors
G	=	coefficient matrix of \dot{q} in aerodynamic state equation	t	=	time, s
H	=	coefficient matrix of q in aerodynamic state equation	V	=	free-stream velocity, m/s
h	=	plunging displacement of airfoil, m	w	=	downwash at three quarters chord point, m/s
I_α	=	mass moment of inertia of airfoil, kg · m	x	=	aeroelastic state vector
K_h	=	linear spring constant per unit span, N/m ²	α	=	pitching angle of airfoil, rad
K_α	=	torsional spring constant per unit span, N/rad	β_i	=	poles in rational function approximation, $i = 1, 2, \dots$
k	=	reduced frequency	ϵ_1, ϵ_2	=	constants in Wagner's function
\mathcal{L}	=	aerodynamic lift on airfoil, N/m	Λ	=	diagonalized aeroelastic system matrix
\mathcal{M}	=	aerodynamic moment on airfoil, N	λ	=	aerodynamic state vector, with components $\lambda_i, i = 1, 2, \dots$
$\bar{M}, \bar{C}, \bar{K}$	=	structural inertia, damping, and stiffness matrices	λ_0	=	inflow velocity, m/s
$\bar{M}, \bar{C}, \bar{K}$	=	generalized inertia, damping, and stiffness matrices	ρ	=	air density, kg/m ³
			Φ	=	left eigenvector matrix
			ϕ	=	Wagner's function
			Ψ	=	right eigenvector matrix
			ω_α, ω_h	=	natural frequencies of airfoil pitching and plunging, rad/s

Presented as Paper 2018-1204 at the 2018 AIAA/ASCE/AHS/ASC Structures, Structural Dynamics, and Materials Conference, Kissimmee, FL, 8–12 January 2018; received 13 March 2018; revision received 12 July 2019; accepted for publication 15 July 2019; published online 9 August 2019. Copyright © 2019 by Xiaochen Hang, Qingguo Fei, and Weihua Su. Published by the American Institute of Aeronautics and Astronautics, Inc., with permission. All requests for copying and permission to reprint should be submitted to CCC at www.copyright.com; employ the eISSN 1533-385X to initiate your request. See also AIAA Rights and Permissions www.aiaa.org/randp.

*Ph.D. Candidate, Department of Engineering Mechanics; also Visiting Ph.D. Student, University of Alabama; hangxiaochen@seu.edu.cn. Student Member AIAA.

†Professor, School of Mechanical Engineering; qgfei@seu.edu.cn.

‡Associate Professor, Department of Aerospace Engineering and Mechanics; suw@eng.ua.edu. Senior Member AIAA.

I. Introduction

AS A new generation entering the field of aerospace engineering research, the authors believe that it is an honor to be able to offer this paper to celebrate Dr. Dewey H. Hodges' 70th birthday. Over decades of research, Dr. Hodges has made outstanding achievements in his research areas of aeroelasticity, geometrically nonlinear beam theory, and rotorcraft dynamics. His leading research has impacted and benefited numerous people in these areas, including the authors of this paper. By taking advantage of this opportunity, the authors would like to present a study that addresses a fundamental aeroelastic

problem, in the hope of bringing new insights into the aeroelastic stability analysis.

In an aeroelastic analysis, mode tracking is a general technique related to eigenvalue problems with varying parameters, such as flight speed and altitude. In general, eigenvalue problems can be classified as either self-adjoint or non-self-adjoint. In self-adjoint problems, the system energy is conserved. However, it is typically a non-self-adjoint problem to solve for the aeroelastic stability boundary [1], where the system energy is not conserved [2]. In an aeroelastic analysis, the vibration frequencies of different modes may change, and mode crossings may occur with the change of airspeed. If such mode crossings are not correctly tracked, it can cause misidentification of the aeroelastic phenomenon, because the observed variations of aeroelastic modes with respect to the varying parameter could be erroneous. When this occurs, the factors leading to aeroelastic instabilities (e.g., flutter and divergence) cannot be adequately understood, and any attempts to improve aircraft performance based on such predictions may be misguided.

In the early years, aeroelastic mode tracking was manually performed based on the analyst's judgment, without applying a robust and automated tracking algorithm. This method is quick but may be daunting and confusing, when frequencies of aeroelastic modes are close in the root locus plane. Desmarais and Bennet [3] proposed an approach for V - g analysis that relied upon the shape of the characteristic polynomial and used the Laguerre's iteration to converge from a previous eigenvalue to the current one. In this method, the increments in reduced frequency must be very small. In addition, this method may fail if the closest zero solution of the characteristic polynomial near the starting point does not correspond to the correct eigenvalue. Van Zyl [4] then improved this method by correlating the modes based on complex inner products between current and previous eigenvalues (with the increment of the parameter, e.g., airspeed), which essentially applied the idea of modal assurance criterion (MAC). Later on, Eldred et al. [2] presented two new methods for mode tracking. One was the complex higher-order eigenpair perturbation (C-HOEP) algorithm, and the other was the complex cross-orthogonality check (C-CORC) method. The first algorithm iteratively computed changes in the eigenpairs due to the parameter perturbations with an important feature of maintaining the correspondence between the baseline and perturbed eigenpairs. The second method, while being similar to Van Zyl's MAC method, was a complex extension of the method developed by Gibson [5]. However, it used the mass bi-orthogonality to reestablish correspondence after a standard reanalysis. By comparing the results of his two methods with those in the previous studies, Eldred et al. recommended C-HOEP and C-CORC in eigenvalue problems of non-self-adjoint systems, such as the aeroelastic flutter analysis using the V - g method, due to the robustness of the two methods. Chen [6] applied a predictor-corrector scheme for the eigenvalue tracking to the g method in flutter analysis. The approach may predict the eigenvalues at the next increment point of the varying parameter by using a linear extrapolation from the eigenvalues and their derivatives at the current increment point. This scheme was also proved to be more robust and less costly than other sorting schemes without using the prediction and correction. Huang et al. [7] tried to deal with the mode tracking jumps to improve the original piecewise quadratic interpolation (PQI) method [8] through shape-preserving cubic spline extrapolation. A fourth-order piecewise polynomial was defined as the shape-preserving interpolation function, and the existing flutter data were used to determine the unknown coefficients.

All these studies have provided significant insights into the aeroelastic mode tracking and are effective on most occasions. However, there are still some disadvantages of the methods when applied in specific studies. One noticeable disadvantage is that small increments of the varying parameter are usually required in most of these methods to track the aeroelastic modes correctly. For example, in perturbation approaches, it is important to take small increments of airspeed to obtain accurate predictions of eigenvalues. Some methods based on splines or interpolation may have difficulties in cases where multiple aeroelastic modes interact within a small frequency neighborhood, which happens commonly in aeroelastic problems of

flexible wing structures. In addition, most of these studies are only validated in specific problems (such as V - g or p - k analysis), modeled by using a specific aerodynamic formulation. In this paper, a different mode tracking method using both left and right eigenvectors is developed to overcome these deficiencies. Mogenier et al. [9] used both left and right eigenvectors of a rotor to track its modes with the varying spin speed. The approach has recently been implemented in MSC.Nastran for the analysis of rotor dynamics [10], where both left and right eigenvectors of the rotor system are employed to track the modes dependent on the rotation rates and to facilitate plotting the Campbell diagram. The rotor dynamics analysis does not involve aeroelastic effects. This paper, however, explores the mode tracking problems of different aeroelastic systems by extending this method.

The remainder of this paper is organized as follows. The theoretical formulation of this study is presented in Sec. II. Several aeroelastic models are introduced briefly in Sec. II.A, where the structural dynamics of a typical 2-D airfoil section is coupled with a frequently used time-domain aerodynamic formulation (such as the Wagner's function, finite-state inflow theory, and rational function approximation). The resulting aeroelastic equations are further transformed into a unified state-space form, where the aeroelastic system matrix is the basis of the mode tracking studies. The unified aeroelastic formulation makes the mode tracking method compatible with various aeroelastic models. Furthermore, in Sec. II.B, the mode tracking algorithm using both left and right eigenvectors of the aeroelastic system matrix is discussed in detail, followed by numerical studies in Sec. III, using the implemented mode tracking method. The numerical cases to be presented include the mode tracking studies on a 2-D airfoil, a linear wing box model, a highly flexible cantilever wing with geometric nonlinearity, and a highly flexible blended-wing-body aircraft with coupled aeroelasticity and flight dynamics. Through the comparison between the new mode tracking method and those that exist in the literature (especially the MAC-based method), advantages and effectiveness of the new method are demonstrated through the studies.

II. Theoretical Formulation

In this section, several aeroelastic formulations are briefly introduced. They are transformed into a unified state-space form, where an orthogonality check using both left and right eigenvectors of the aeroelastic systems is applied to track aeroelastic modes in the stability analysis.

A. Generalized Aeroelastic Equations of Motion

A 2-D rigid airfoil section is shown in Fig. 1 with a plunging degree-of-freedom h and a pitching degree-of-freedom α . Its equation of motion is given by

$$\begin{bmatrix} m & S_\alpha \\ S_\alpha & I_\alpha \end{bmatrix} \begin{Bmatrix} \ddot{h}(t) \\ \ddot{\alpha}(t) \end{Bmatrix} + \begin{bmatrix} K_h & 0 \\ 0 & K_\alpha \end{bmatrix} \begin{Bmatrix} h(t) \\ \alpha(t) \end{Bmatrix} = \begin{Bmatrix} -\mathcal{L}(t) \\ \mathcal{M}(t) \end{Bmatrix} \quad (1)$$

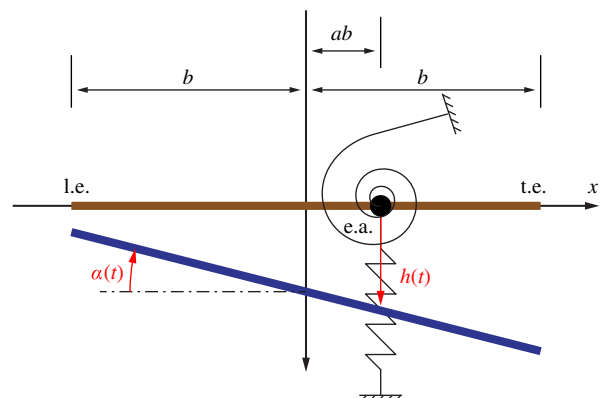


Fig. 1 A 2-D rigid airfoil section.

where m , S_{α} , and I_{α} are the total mass, structural imbalance, and mass moment of inertia of the airfoil, respectively. K_h and K_{α} are the linear and torsional spring constants, respectively. \mathcal{L} and \mathcal{M} are aerodynamic force and moment at the elastic axis, respectively. Finally, the structural damping is not considered for this airfoil for simplicity.

To apply the proposed mode tracking method in aeroelastic stability analysis, one may transform Eq. (1) into the state-space form. In addition, this paper aims at developing a mode tracking approach that can accommodate different unsteady aerodynamic formulations to determine the loads \mathcal{L} and \mathcal{M} , as well as the aerodynamic state differential equations. In doing so, several frequently used unsteady aerodynamic formulations are considered in this paper.

1. Wagner's Function

Wagner's function is used to model the indicial response of the aerodynamic loads under a sudden change of downwash. As the time history of the downwash can be approximated by the sum of several step signals, the unsteady aerodynamic loads under an arbitrary airfoil motion can be derived by the Duhamel's integral, given by

$$\begin{aligned} \mathcal{L} &= \pi\rho b^2(\ddot{h} + V\dot{\alpha} - ab\ddot{\alpha}) \\ &\quad + 2\pi\rho bV\left(w(0)\phi(t) + \int_0^t \frac{\partial w(\tau)}{\partial \tau} \phi(t-\tau) d\tau\right) \\ \mathcal{M} &= \pi\rho b^2\left[ab\ddot{h} - \left(\frac{1}{2} - a\right)bV\dot{\alpha} - \left(\frac{1}{8} + a^2\right)b^2\ddot{\alpha}\right] \\ &\quad + 2\pi\rho b^2V\left(\frac{1}{2} + a\right)\left(w(0)\phi(t) + \int_0^t \frac{\partial w(\tau)}{\partial \tau} \phi(t-\tau) d\tau\right) \end{aligned} \quad (2)$$

where $w(t)$ is the downwash at the three-quarters chord, given by

$$w(t) = \dot{h}(t) + \left(\frac{1}{2} - a\right)b\dot{\alpha}(t) + V\alpha(t) \quad (3)$$

and the Wagner's function $\phi(t)$ may take the approximate form of

$$\phi(t) = 1 - C_1 e^{-\varepsilon_1(V/b)t} - C_2 e^{-\varepsilon_2(V/b)t} \quad (4)$$

where $C_1 = 0.165$, $C_2 = 0.335$, $\varepsilon_1 = 0.0455$, and $\varepsilon_2 = 0.3$ [11]. The integrals in Eq. (2) are transformed by using integration by parts, leading to

$$\begin{aligned} \mathcal{L} &= \pi\rho b^2(\ddot{h} + V\dot{\alpha} - ab\ddot{\alpha}) \\ &\quad + 2\pi\rho bV\left(w(t)\phi(0) - \int_0^t w(\tau) \frac{\partial \phi(t-\tau)}{\partial \tau} d\tau\right) \\ \mathcal{M} &= \pi\rho b^2\left[ab\ddot{h} - \left(\frac{1}{2} - a\right)bV\dot{\alpha} - \left(\frac{1}{8} + a^2\right)b^2\ddot{\alpha}\right] \\ &\quad + 2\pi\rho b^2V\left(\frac{1}{2} + a\right)\left(w(t)\phi(0) - \int_0^t w(\tau) \frac{\partial \phi(t-\tau)}{\partial \tau} d\tau\right) \end{aligned} \quad (5)$$

The integrals in Eq. (5) are defined as a summation of two individual aerodynamic states, λ_1 and λ_2 , given by

$$\begin{aligned} \lambda_1 &= C_1 \varepsilon_1 \frac{V}{b} \int_0^t w(\tau) e^{-\varepsilon_1(V/b)(t-\tau)} d\tau \\ \lambda_2 &= C_2 \varepsilon_2 \frac{V}{b} \int_0^t w(\tau) e^{-\varepsilon_2(V/b)(t-\tau)} d\tau \\ \lambda_1 + \lambda_2 &= - \int_0^t w(\tau) \frac{\partial \phi(t-\tau)}{\partial \tau} d\tau \end{aligned} \quad (6)$$

To simplify the equations, one can define the airfoil motion and complete state vector as

$$\begin{aligned} \mathbf{q} &= \{h \quad \alpha\}^T \\ \boldsymbol{\lambda} &= \{\lambda_1 \quad \lambda_2\}^T \end{aligned} \quad (7)$$

Obviously, the aerodynamic lift and moment are both functions of airfoil motion \mathbf{q} , its time derivatives ($\dot{\mathbf{q}}$ and $\ddot{\mathbf{q}}$), as well as the aerodynamic state $\boldsymbol{\lambda}$, that is,

$$\begin{Bmatrix} \mathcal{L} \\ \mathcal{M} \end{Bmatrix} = \mathbf{M}_A \ddot{\mathbf{q}} + \mathbf{C}_A \dot{\mathbf{q}} + \mathbf{K}_A \mathbf{q} + \mathbf{D} \boldsymbol{\lambda} \quad (8)$$

where

$$\begin{aligned} \mathbf{M}_A &= \pi\rho b^2 \begin{bmatrix} 1 & -ab \\ ab & -\left(\frac{1}{8} + a^2\right)b^2 \end{bmatrix} \\ \mathbf{C}_A &= \pi\rho bV \begin{bmatrix} 2\phi(0) & b + 2\left(\frac{1}{2} - a\right)b\phi(0) \\ 2\left(\frac{1}{2} + a\right)b\phi(0) & -\left(\frac{1}{2} - a\right)b^2 + 2\left(\frac{1}{4} - a^2\right)b^2\phi(0) \end{bmatrix} \\ \mathbf{K}_A &= 2\pi\rho bV^2 \begin{bmatrix} 0 & \phi(0) \\ 0 & \left(\frac{1}{2} + a\right)b\phi(0) \end{bmatrix} \\ \mathbf{D} &= 2\pi\rho bV \begin{bmatrix} 1 & 1 \\ \left(\frac{1}{2} + a\right)b & \left(\frac{1}{2} + a\right)b \end{bmatrix} \end{aligned} \quad (9)$$

One can further take the time derivatives of λ_1 and λ_2 in Eq. (6) to set up the aerodynamic state differential equation, given by

$$\begin{aligned} \dot{\lambda}_1 &= -\varepsilon_1 \frac{V}{b} \lambda_1 + C_1 \varepsilon_1 \frac{V}{b} \left[\dot{h} + \left(\frac{1}{2} - a\right)b\dot{\alpha} + V\alpha\right] \\ \dot{\lambda}_2 &= -\varepsilon_2 \frac{V}{b} \lambda_2 + C_2 \varepsilon_2 \frac{V}{b} \left[\dot{h} + \left(\frac{1}{2} - a\right)b\dot{\alpha} + V\alpha\right] \end{aligned} \quad (10)$$

where $\dot{h}(0) = 0$, $\dot{\alpha}(0) = 0$, and $\alpha(0) = 0$. Eq. (10) can be written in the matrix form of

$$\dot{\boldsymbol{\lambda}} = \mathbf{E} \boldsymbol{\lambda} + \mathbf{F} \ddot{\mathbf{q}} + \mathbf{G} \dot{\mathbf{q}} + \mathbf{H} \mathbf{q} \quad (11)$$

where

$$\begin{aligned} \mathbf{E} &= \begin{bmatrix} -\varepsilon_1 \frac{V}{b} & 0 \\ 0 & -\varepsilon_2 \frac{V}{b} \end{bmatrix}, \quad \mathbf{F} = \mathbf{0}_{2 \times 2}, \\ \mathbf{G} &= \begin{bmatrix} C_1 \varepsilon_1 \frac{V}{b} & C_1 \varepsilon_1 V \left(\frac{1}{2} - a\right) \\ C_2 \varepsilon_2 \frac{V}{b} & C_2 \varepsilon_2 V \left(\frac{1}{2} - a\right) \end{bmatrix}, \quad \mathbf{H} = \begin{bmatrix} 0 & C_1 \varepsilon_1 \frac{V^2}{b} \\ 0 & C_2 \varepsilon_2 \frac{V^2}{b} \end{bmatrix} \end{aligned} \quad (12)$$

To complete the aeroelastic equation, one can substitute Eq. (8) into Eq. (1) and combine with Eq. (11), yielding

$$\begin{aligned} \bar{\mathbf{M}} \ddot{\mathbf{q}} + \bar{\mathbf{C}} \dot{\mathbf{q}} + \bar{\mathbf{K}} \mathbf{q} &= \mathbf{D} \boldsymbol{\lambda} \\ \dot{\boldsymbol{\lambda}} &= \mathbf{E} \boldsymbol{\lambda} + \mathbf{F} \ddot{\mathbf{q}} + \mathbf{G} \dot{\mathbf{q}} + \mathbf{H} \mathbf{q} \end{aligned} \quad (13)$$

where the generalized aeroelastic matrices, $\bar{\mathbf{M}}$, $\bar{\mathbf{C}}$, and $\bar{\mathbf{K}}$, are obtained by combining the structural matrices in Eq. (1), with the corresponding aerodynamic matrices in Eq. (9).

2. Finite-State Inflow Theory

The second time-domain unsteady aerodynamic formulation considered in this paper is the finite-state inflow theory developed by Peters and co-workers [12–14]. It calculates aerodynamic loads on a thin airfoil section in incompressible inviscid flow. The lift and moment of a thin 2-D airfoil section about the elastic axis are given by

$$\begin{aligned}
\mathcal{L} &= \pi\rho b^2(\ddot{h} + V\dot{\alpha} - ab\ddot{\alpha}) \\
&\quad + 2\pi\rho bV^2\left[\alpha + \frac{\dot{h}}{V} + \left(\frac{1}{2} - a\right)b\frac{\dot{\alpha}}{V} - \frac{\lambda_0}{V}\right] \\
\mathcal{M} &= \pi\rho b^2\left[ab\ddot{h} - \left(\frac{1}{2} - a\right)bV\dot{\alpha} - \left(\frac{1}{8} + a^2\right)b^2\ddot{\alpha}\right] \\
&\quad + 2\pi\rho b^2V^2\left(\frac{1}{2} + a\right)\left[\alpha + \frac{\dot{h}}{V} + \left(\frac{1}{2} - a\right)b\frac{\dot{\alpha}}{V} - \frac{\lambda_0}{V}\right] \quad (14)
\end{aligned}$$

where the inflow parameter λ_0 accounts for induced flow due to the free vorticity, which is the weighted summation of the inflow states λ as described in Peters and Johnson [12], that is,

$$\lambda_0 = \frac{1}{2} \sum_{i=1}^N \bar{b}_i \lambda_i \quad (15)$$

where N is the number of inflow states defined on the airfoil, and \bar{b} are coefficients that can be obtained by the least-square method [13].

Even though the aerodynamic states are defined differently, Eq. (14) can still be written in a similar form as Eq. (8), whereas the aerodynamic matrices are given by

$$\begin{aligned}
\mathbf{M}_A &= \pi\rho b^2 \begin{bmatrix} 1 & -ab \\ ab & -\left(\frac{1}{8} + a^2\right)b^2 \end{bmatrix} \\
\mathbf{C}_A &= 2\pi\rho bV \begin{bmatrix} 1 & (1-a)b \\ \left(\frac{1}{2} + a\right)b & \left(\frac{1}{2} - a\right)ab^2 \end{bmatrix} \\
\mathbf{K}_A &= 2\pi\rho bV \begin{bmatrix} 0 & V \\ 0 & \left(\frac{1}{2} + a\right)bV \end{bmatrix} \\
\mathbf{D} &= -\pi\rho bV \begin{bmatrix} \bar{b}_1 & \bar{b}_2 & \cdots & \bar{b}_N \\ \left(\frac{1}{2} + a\right)b\bar{b}_1 & \left(\frac{1}{2} + a\right)b\bar{b}_2 & \cdots & \left(\frac{1}{2} + a\right)b\bar{b}_N \end{bmatrix} \quad (16)
\end{aligned}$$

Additionally, the governing equation for the inflow states is

$$\bar{\mathbf{W}}\dot{\lambda} + \frac{V}{b}\lambda = \bar{\mathbf{c}}\left[\ddot{h} + \left(\frac{1}{2} - a\right)b\ddot{\alpha} + V\dot{\alpha}\right] \quad (17)$$

where the coefficients $\bar{\mathbf{W}}$ and $\bar{\mathbf{c}}$ are both defined in Peters et al. [13]. Equation (17) can be conveniently transformed into the same form as Eq. (11), with different definitions of the coefficient matrices \mathbf{E} , \mathbf{F} , \mathbf{G} , and \mathbf{H} , given by

$$\begin{aligned}
\mathbf{E} &= \bar{\mathbf{W}}^{-1} \left[\text{diag}\left(-\frac{V}{b}\right) \right]_{N \times N} & \mathbf{F} &= \bar{\mathbf{W}}^{-1} \left[\bar{\mathbf{c}} \left(\frac{1}{2} - a\right)b\bar{\mathbf{c}} \right] \\
\mathbf{G} &= \bar{\mathbf{W}}^{-1} \left[\mathbf{0}_{N \times 1} \quad V\bar{\mathbf{c}} \right]_{N \times N} & \mathbf{H} &= \mathbf{0}_{N \times N} \quad (18)
\end{aligned}$$

With the details omitted, one can demonstrate that the aeroelastic equation with the finite-state inflow theory still falls in the same generalized form as Eq. (13).

3. Unsteady Aerodynamics with Rational Functions

The rational function approximation (RFA) [15,16] can be used to transfer frequency-dependent aerodynamic loads into the time domain. The aeroelastic equation in the Laplace domain is given by

$$(\mathbf{M}s^2 + \mathbf{K})\mathbf{q}(s) = \frac{1}{2}\rho V^2 \mathbf{Q}(s)\mathbf{q}(s) \quad (19)$$

where s is the Laplace variable. $\mathbf{Q}(s)$ is the approximation to the aerodynamic influence coefficient (AIC) matrix. With the Roger's approximation [17], $\mathbf{Q}(s)$ is given by

$$\mathbf{Q}(s) = \mathbf{A}_0 + \mathbf{A}_1 \frac{sb}{V} + \mathbf{A}_2 \left(\frac{sb}{V}\right)^2 + \sum_{i=1}^N \left(\mathbf{A}_{i+2} \frac{s}{s + \frac{V}{b}\beta_i}\right) \quad (20)$$

where the first three entries represent the quasi-steady aerodynamic load, while the remaining items in summation account for the lag behavior of unsteady aerodynamic load. All the \mathbf{A}_i are unknown coefficients that can be determined through the least square fitting [16]. Once the unknown coefficients are determined, Eq. (19) can be transformed to the time domain as

$$\begin{aligned}
\mathbf{M}\ddot{\mathbf{q}}(t) + \mathbf{K}\mathbf{q}(t) &= \frac{1}{2}\rho V^2 \mathbf{A}_0 \mathbf{q}(t) + \frac{1}{2}\rho V^2 \left(\frac{b}{V}\right) \mathbf{A}_1 \dot{\mathbf{q}}(t) \\
&\quad + \frac{1}{2}\rho V^2 \left(\frac{b}{V}\right)^2 \mathbf{A}_2 \ddot{\mathbf{q}}(t) + \sum_{i=1}^N \left(\frac{1}{2}\rho V^2 \mathbf{A}_{i+2} \lambda_i\right) \quad (21)
\end{aligned}$$

which is rewritten as

$$\begin{aligned}
\left(\mathbf{M} - \frac{1}{2}\rho V^2 \left(\frac{b}{V}\right)^2 \mathbf{A}_2\right) \ddot{\mathbf{q}}(t) + \left(-\frac{1}{2}\rho V^2 \frac{b}{V} \mathbf{A}_1\right) \dot{\mathbf{q}}(t) \\
+ \left(\mathbf{K} - \frac{1}{2}\rho V^2 \mathbf{A}_0\right) \mathbf{q}(t) = \sum_{i=1}^N \left(\frac{1}{2}\rho V^2 \mathbf{A}_{i+2} \lambda_i\right) \quad (22)
\end{aligned}$$

where the augmented states λ_i are defined by

$$\dot{\lambda}_i(s) = \frac{s}{s + \frac{V}{b}\beta_i} \mathbf{q}(s), \quad (i = 1, 2, \dots, N) \quad (23)$$

which is transformed to the time domain, resulting in the governing differential equation for the aerodynamic states

$$\dot{\lambda}_i = -\frac{V}{b}\beta_i \lambda_i + \dot{\mathbf{q}}, \quad (i = 1, 2, \dots, N) \quad (24)$$

Equations (22) and (24), after being combined to form the aeroelastic equation, can be easily written into the generalized form of Eq. (13). In addition to the RFA, there are other approaches (e.g., minimum-state RFA [18], p-transform [19,20], and FAMUSS [21]) that can be applied to generate reduced-order aerodynamic models and build state-space formulations for aeroelastic and aeroservoelastic studies. A good summary on various methods and a comparison on their advantages and disadvantages in aeroelastic studies were provided in [22,23]. The RFA is chosen in the current study due to its simplicity in deriving the generalized aeroelastic equation in the form of Eq. (13).

4. Aeroelastic Formulation for Flexible Wings with 2-D Aerodynamics

The previous discussions on the aeroelastic formulations were all based on 2-D airfoils. However, it does not prevent one from applying these aerodynamic theories to analyze flexible wings, where recent research activities can be found in the literature. Palacios et al. [24] provided a summary of aeroelastic modeling for flexible wings. For most formulations, one may still reach the aeroelastic equations in a form of

$$\begin{aligned}
\mathbf{M}\ddot{\mathbf{q}} + \mathbf{C}\dot{\mathbf{q}} + \mathbf{K}\mathbf{q} &= \mathbf{R}(\ddot{\mathbf{q}}, \dot{\mathbf{q}}, \mathbf{q}, \lambda) \\
\dot{\lambda} &= \mathbf{E}\lambda + \mathbf{F}\ddot{\mathbf{q}} + \mathbf{G}\dot{\mathbf{q}} + \mathbf{H}\mathbf{q} \quad (25)
\end{aligned}$$

where \mathbf{q} are the elastic degrees of freedom and λ are the aerodynamic states. \mathbf{R} is the aerodynamic load vector as a function of the elastic degrees and the aerodynamic states. The coefficient matrices of aerodynamic states \mathbf{E} , \mathbf{F} , \mathbf{G} , and \mathbf{H} should be determined according to the applied unsteady aerodynamic theory when setting up the aeroelastic equation.

B. Orthogonality Check Method Using Left and Right Eigenvectors

If the problem described by Eq. (25) is geometrically nonlinear, the inertia, damping, and stiffness matrices (\bar{M} , \bar{C} , and \bar{K}) may also be functions of the elastic degrees of freedom. To find the stability boundary of such a nonlinear system, one needs to linearize the equation about a nonlinear equilibrium state under a given parameter (e.g., airspeed) as shown in Su and Cesnik [25]. However, this process is not required for linear problems. The linear or linearized aeroelastic equation can be reorganized with all terms of the same variables collected together, resulting in

$$\begin{aligned} \bar{M}\ddot{q} + \bar{C}\dot{q} + \bar{K}q &= D\lambda \\ \dot{\lambda} &= E\lambda + F\ddot{q} + G\dot{q} + Hq \end{aligned} \quad (26)$$

where \bar{M} , \bar{C} , and \bar{K} are generalized inertia, damping, and stiffness matrices, respectively. Equation (26) may be further written into the state-space form as

$$\dot{x} = Ax \quad (27)$$

where

$$A = \begin{bmatrix} I & 0 & 0 \\ 0 & \bar{M} & 0 \\ 0 & -F & I \end{bmatrix}^{-1} \begin{bmatrix} 0 & I & 0 \\ -\bar{K} & -\bar{C} & D \\ H & G & E \end{bmatrix} \quad (28)$$

Let A be the system matrix of an aeroelastic system at a given airspeed, which is, in general, not symmetric in aeroelastic problems. According to the eigendecomposition theory (also called spectral decomposition), A can be diagonalized if it has no repeated eigenvalues, given by

$$A = \Psi\Lambda\Phi^H \quad (29)$$

where Λ is a diagonal matrix, and

$$\Phi^H = \Psi^{-1} \quad (30)$$

The operator $(\cdot)^H$ is the conjugate transpose or Hermitian transpose. Postmultiplying $(\Phi^H)^{-1} = \Psi$ on both sides of Eq. (29) yields

$$A\Psi = \Psi\Lambda \quad (31)$$

which is essentially a right eigenvalue problem of A . The diagonal entries of Λ are the eigenvalues. Each column of Ψ corresponds to a right eigenvector of A . Similarly, one can premultiply $\Phi^H = \Psi^{-1}$ on both sides of Eq. (29), resulting in

$$\Phi^H A = \Lambda\Phi^H \quad (32)$$

which is essentially a left eigenvalue problem of A . Here, each row of Φ^H is the left eigenvector of the corresponding eigenvalue of A . Therefore, the left and right eigenvector matrices of A can be used to diagonalize the system matrix by following Eq. (29). In addition, the two eigenvector matrices are orthogonal to each other, that is,

$$\Phi^H\Psi = I \quad (33)$$

which is apparent according to Eq. (30).

Such a bi-orthogonal relation can be applied to track the aeroelastic modes with a varying airspeed. At two consecutive airspeed increments (V_i and V_{i+1}), the aeroelastic systems are denoted as

$$\begin{aligned} A_i &= \Psi_i\Lambda_i\Phi_i^H \\ A_{i+1} &= \Psi_{i+1}\Lambda_{i+1}\Phi_{i+1}^H \end{aligned} \quad (34)$$

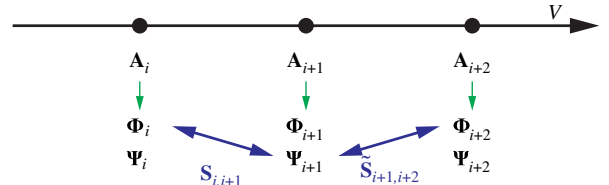


Fig. 2 Scheme of orthogonality check using both left and right eigenvectors.

The matrix for checking orthogonality of the aeroelastic modes can be defined as

$$S_{i,i+1} \triangleq \Phi_i^H\Psi_{i+1} \quad (35)$$

Equation (35) is similar to Eq. (33), yet with the left and right eigenvectors evaluated at two different airspeeds. If the speed increment ΔV is not significantly large, the bi-orthogonal relation is approximately maintained [4]. That is, $S_{i,i+1}$ is a diagonally dominant matrix [2] if the modes are properly sorted, even though it is no longer an identity matrix. One may define a similar orthogonality checking matrix as

$$\tilde{S}_{i,i+1} \triangleq \Psi_i^H\Phi_{i+1} \quad (36)$$

which is also diagonally dominant. One can take advantage of both Eqs. (35) and (36) when implementing the current mode tracking method. The scheme is briefly illustrated in Fig. 2. If the modes of system A_i are already sorted, the modes of A_{i+1} can be tracked using the sorted left eigenvector matrix Φ_i (of A_i) and the right eigenvector matrix Ψ_{i+1} (of A_{i+1}). In the sorting process, the columns of Ψ_{i+1} are reordered to make the product $(\Phi_i^H \cdot \Psi_{i+1})$ a diagonally dominant matrix. At the next speed increment to track the modes of system A_{i+2} , one can use the previously sorted right eigenvector matrix Ψ_{i+1} , while involving the left eigenvector matrix Φ_{i+2} (of A_{i+2}). In this sorting process, the columns of Φ_{i+2} are then reordered to make $(\Psi_{i+1}^H \cdot \Phi_{i+2})$ diagonally dominant. By implementing this scheme, one only has to solve for either left or right eigenvectors of the aeroelastic system at one airspeed increment, which reduces the overall calculation expense for the mode tracking.

The mode tracking method developed in this paper is based on the eigendecomposition theory [or Eq. (29)] that is true as long as the system (either self-adjoint or non-self-adjoint) has no repeated eigenvalues. Consequently, it is also true for non-self-adjoint aeroelastic systems under all airspeed, where the left and right eigenvectors of the system are always orthogonal. Therefore, the orthogonality checking matrices S and \tilde{S} are diagonally dominant, even when the airspeed is about the flutter boundary. In the following numerical studies, the mode tracking method discussed above is compared with the method using MAC values between the right eigenvectors of the aeroelastic systems, where the orthogonality checking criterion is

$$T_{i,i+1} \triangleq \Psi_i^H\Psi_{i+1} \quad (37)$$

Note that the right eigenvectors of the aeroelastic system are not always orthogonal, as the system is non-self-adjoint, which brings difficulty to the mode tracking using such a MAC-based method in some cases.

III. Numerical Studies

Numerical studies on aeroelastic mode tracking are presented in this section, where the new approach using both left and right eigenvectors for orthogonality check is compared with other methods. The advantages of this approach are highlighted from cases with a linear aeroelastic problem, a geometrically nonlinear aeroelastic problem, and a coupled aeroelastic and flight dynamic problem, respectively.

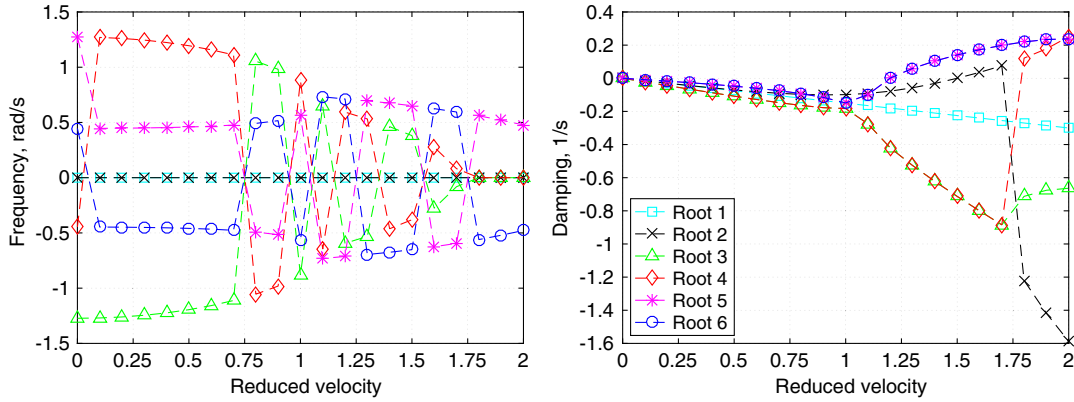


Fig. 3 Frequency and damping vs reduced velocity of 2-D airfoil (no sort).

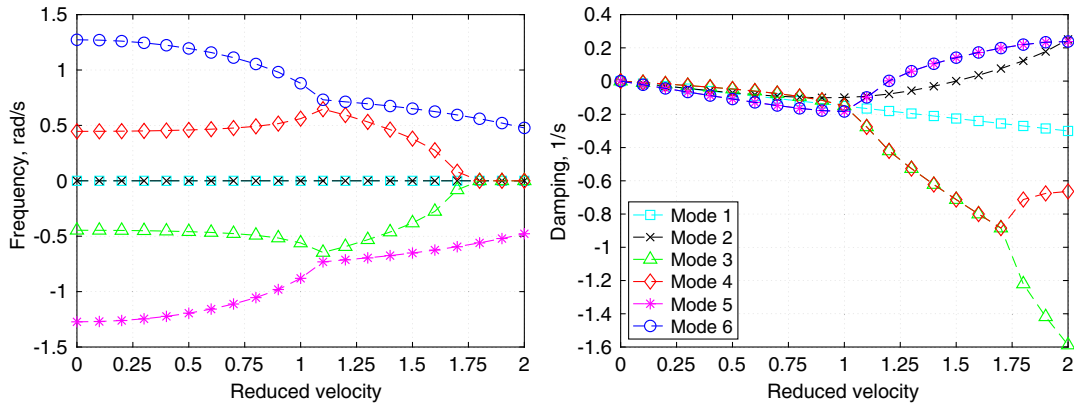


Fig. 4 Frequency and damping vs reduced velocity of 2-D airfoil (sorted).

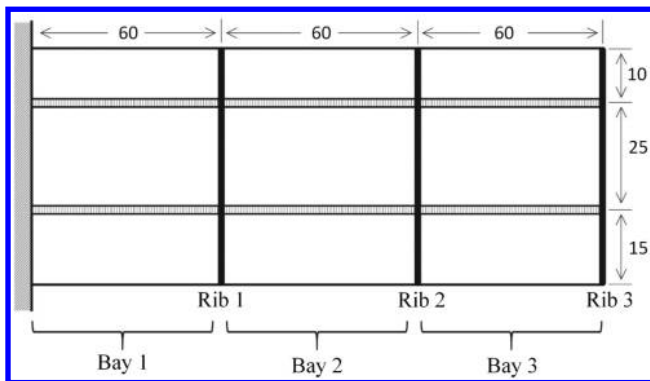


Fig. 5 Geometry of rectangular wing box (unit in inches).

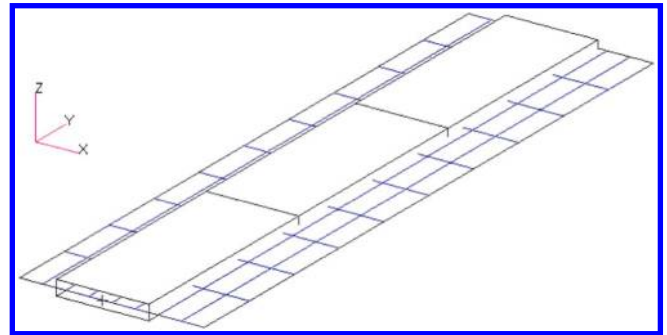


Fig. 6 FEM and aerodynamic model of rectangular wing box.

A. Two-Dimensional Airfoil

A 2-D airfoil (refer to Fig. 1) is studied in this case, whose parameters are nondimensionalized as follows: $a = -0.3$, $\omega_h/\omega_\alpha = 0.5$, $S_a/mb = 0.2$, $\sqrt{I_a/mb^2} = 0.3$, and $m/\pi\rho b^2 = 10$. The unsteady aerodynamic loads on the airfoil are calculated using the Theodorsen’s formula, with a one-term Padé approximation. Eigenvalues of the aeroelastic system are solved as a function of the reduced velocity, $\bar{V} = V/b\omega_\alpha$. Figure 3 plots the aeroelastic frequency and damping extracted from the eigenvalues. All the curves in Fig. 3 are generated based on the roots from the flutter

Table 1 Material properties of rectangular wing box

Property	Value
Young’s modulus, E	10.5×10^6 psi
Shear modulus, G	4.0×10^6 psi
Density, ρ	2.633×10^{-4} slug/in. ³

determinant at each reduced velocity without sorting. It can be seen that the solution effectively finds the flutter point ($V_f = 1.2$). Several roots cross with each other, where the cause of the mode crossings in this sample is attributed to the numerical scheme that finds the roots of the flutter determinant. In complicated problems, however, aeroelastic mode crossing may cause misunderstanding of the flutter mechanism. For such a simple case, all aeroelastic modes can be easily identified, and the figures can be revised to reflect the sorted modes (see Fig. 4). However, such work is never straightforward for complicated aeroelastic systems, as discussed in Sec. I. Therefore, it is of great importance to sort and track these roots properly and efficiently.

B. Linear Wing Box Model

The wing model studied in this case is illustrated in Fig. 5. It is an unswept cantilever wing with a constant cross section. The material properties of the wing box model are listed in Table 1. The finite element model (created in MSC.Nastran) of this wing box model is shown in Fig. 6. There are three bays in this wing box model. For each bay, there are two skin elements, two spar webs, and one rib. There are

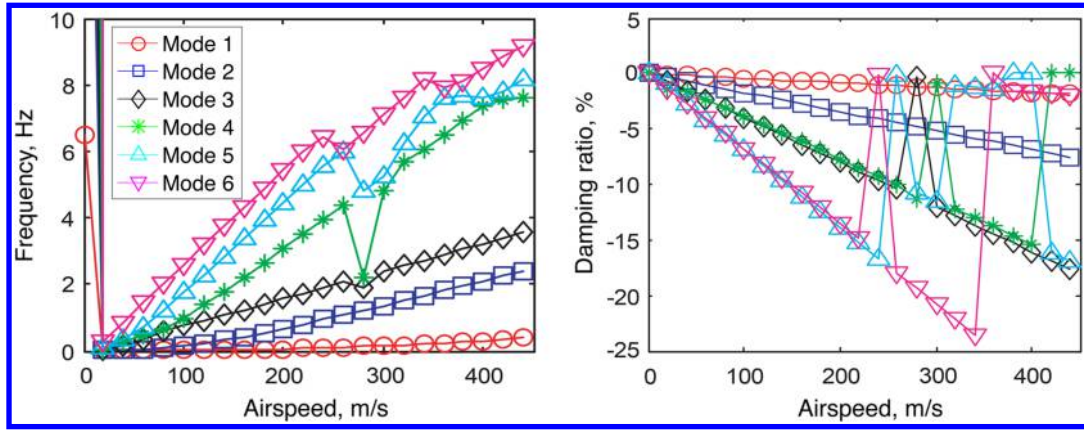


Fig. 7 Frequency (left) and damping ratio (right) vs airspeed (no sort).

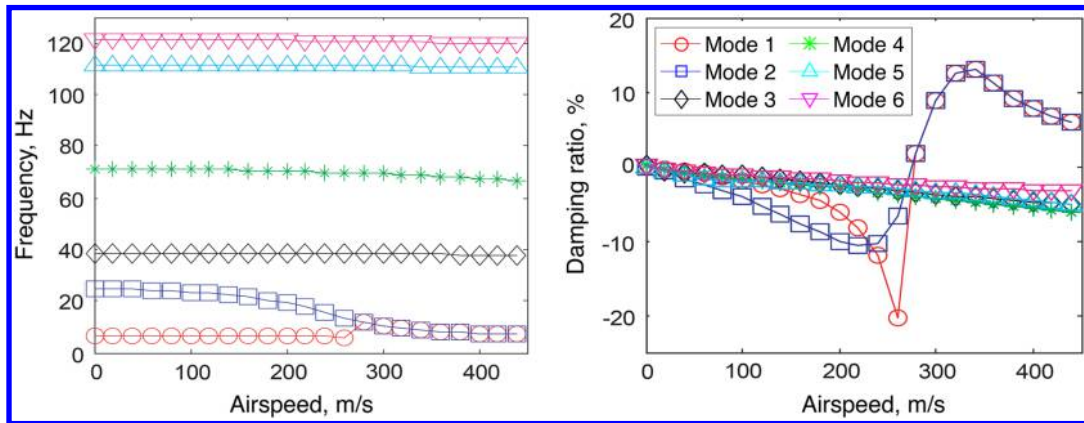


Fig. 8 Frequency (left) and damping ratio (right) vs airspeed using MAC method, $\Delta V = 20$ m/s.

four spar caps modeled by axial rod elements in each bay. This wing box model was originally studied by Rudisill and Bhatia [26] and later by McIntosh and Ashley [27], as well as other researchers [28,29]. A mode tracking study on this wing model was performed in [30]. The results of that study are repeated herein for completeness and to compare with the mode tracking method using both the left and right eigenvectors.

The unsteady aerodynamic loads are established through the doublet lattice method (DLM) implemented in MSC.Nastran. M , K , and the aerodynamic influence coefficient matrix Q in a range of reduced frequency k are extracted from MSC.Nastran. Because the aeroelastic model is linear, the linearization process described in the previous section is unnecessary. After applying the rational function approximation approach, the aeroelastic equation in the state-space form can be obtained. The aeroelastic stability analysis is carried out by solving the eigenvalue problem of system matrix A .

When the eigenvalues are just sorted by the imaginary part (frequency) in ascending order, six modes that have the smallest

imaginary parts are selected to be plotted without applying any mode tracking technique, as shown in Fig. 7. Mode crossing occurs in these plots, and the trends of natural frequencies and damping ratios are not correctly tracked. However, these modes are aerodynamic dominant, and they do not help to understand the real mechanism of the aeroelastic instability. Figure 8 shows the frequency and damping ratio of the first six elastic modes, where the mode tracking is performed by checking the modal assurance criterion (MAC) numbers of the aeroelastic systems' right eigenvectors (named as "MAC method" in this paper). The damping ratio of the second mode (a torsional mode) crosses the zero-line at the airspeed of $V = 273$ m/s, which implies the onset of flutter. This flutter speed is similar to the one (267 m/s) reported by Striz and Venkayya [29]. Even though the mode tracking result appears to be reasonable, the first mode is inaccurately tracked regarding both the frequency and damping ratio. The first mode is estimated to merge with the second mode after the airspeed $V = 280$ m/s, which is shown and proved to be erroneous in the following discussion. The error is attributed to a

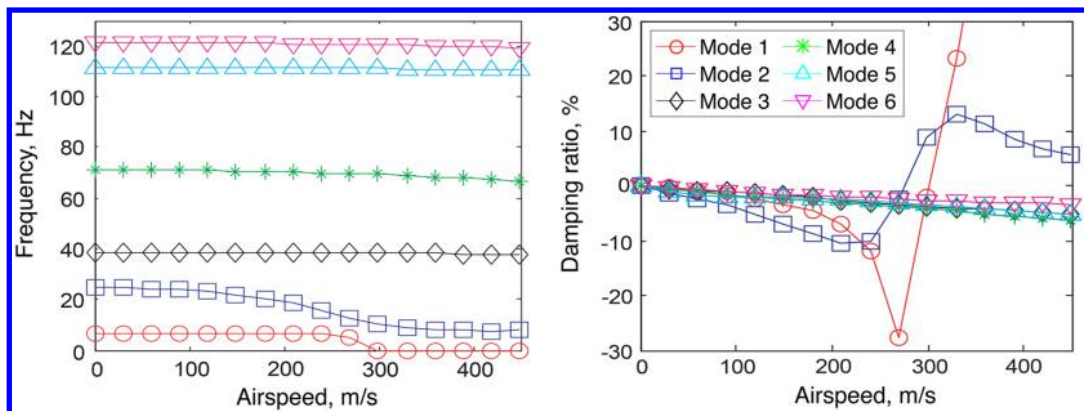


Fig. 9 Frequency (left) and damping ratio (right) vs airspeed using current orthogonality check method, $\Delta V = 30$ m/s.

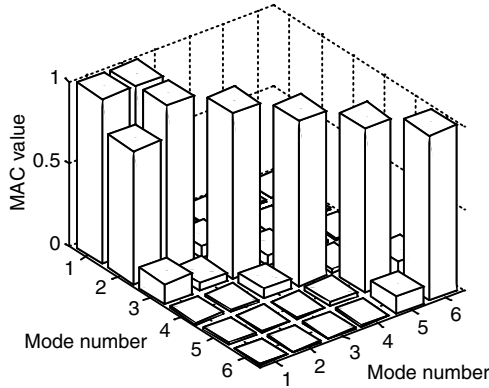


Fig. 10 Normalized orthogonality coefficient using MAC method.

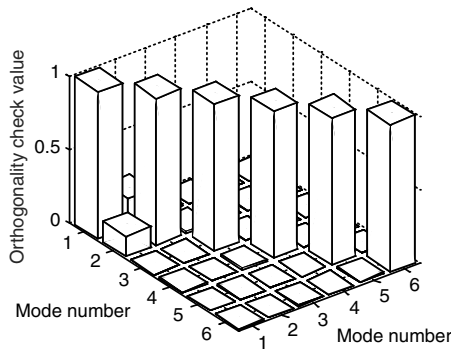


Fig. 11 Normalized orthogonality coefficient using current method.

Table 2 Properties of highly flexible wing

Property	Value
Span	16 m
Chord	1 m
Spanwise ref. axis location (from l.e.)	50% of chord
Center of gravity (from l.e.)	50% of chord
Flat bending rigidity	$2 \times 10^4 \text{ N} \cdot \text{m}^2$
Chord bending rigidity	$4 \times 10^6 \text{ N} \cdot \text{m}^2$
Torsional rigidity	$1 \times 10^4 \text{ N} \cdot \text{m}^2$
Mass per unit span	0.75 kg/m
Rotational inertia per unit span	0.1 kg · m

shortcoming of the MAC-based method that is also discussed later in detail.

Nonetheless, if the orthogonality check method using both left and right eigenvectors is applied, every mode can be separated as shown in Fig. 9. The frequency versus airspeed plot indicates that the aeroelastic divergence occurs as the first modal frequency goes to

zero at airspeed 301 m/s, which is also very close to the results from Striz and Venkayya [29]. In addition, the orthogonality check method has robust effectiveness even when the speed increment is relatively large (here $\Delta V = 30 \text{ m/s}$). However, other mode tracking methods, including the MAC method and perturbation methods, usually require a smaller airspeed increment to ensure the solution accuracy, which indicates a more substantial computation expense.

It can be noted that the data plotted in Figs. 8 and 9 both come from eigenvalue analysis of the same aeroelastic system, except that the MAC method only uses the right eigenvectors. It is because of this reason that the MAC method is not able to identify the aeroelastic mode near the flutter point. Figures 10 and 11 plot the entries of the orthogonality checking matrices using the MAC method and the method based on left and right eigenvectors, respectively, where the advantage of latter one is highlighted. For a non-self-adjoint system, such as aeroelastic systems, the right eigenvectors are no longer orthogonal to each other. When the system is at an airspeed close to the flutter point (here $V = 280 \text{ m/s}$), the off-diagonal entries are large enough to preclude the clear mode separation as shown in Fig. 10. With similar MAC values, the MAC method fails to identify the two modes. On the other hand, the mode tracking method based on left and right eigenvectors is much more effective because the orthogonality is maintained between the left and right eigenvectors at an airspeed close to the flutter point, as shown in Fig. 11. The diagonal entries in this figure are always dominant.

C. Highly Flexible Cantilever Wing

In this case, the mode tracking method introduced in this paper is tested with a geometrically nonlinear aeroelastic system. By following the approach described in [25], the aeroelastic stability analysis of a slender wing is carried out, whose properties are listed in Table 2. The wing is discretized into eight strain-based nonlinear beam finite elements (refer to Su and Cesnik [31] for the beam formulation), coupled with the finite-state unsteady aerodynamics. The air density is 0.088 kg/m^3 at the 20,000 m altitude.

With a cantilevered boundary condition and a root pitch angle of 2° , stability of the aeroelastic system is evaluated within the free stream velocity range between 1 and 35 m/s, with an increment of 1 m/s. From the root locus plot (Fig. 12), the flutter boundary is identified as 23.2 m/s with a frequency of 10.2 rad/s. However, the root loci of several modes are very close to each other, which makes it inconvenient to track all these modes directly from Fig. 12. Individual aeroelastic modes are tracked by using the method with orthogonality check discussed in this paper. Figure 13 plots the frequency and damping ratio of some aeroelastic modes around the flutter point, while Fig. 14 includes modes in a wider frequency range. It is not a surprise that Fig. 13 predicts the same flutter boundary as the root locus plot does. The orthogonality of the aeroelastic modes is checked at preflutter speeds (22 and 23 m/s). Figure 15 is the orthogonality coefficient matrix when the modes are sorted by using the MAC-based method. It is noticeable that there are many large off-diagonal values in Fig. 15, which means that some modes may be incorrectly tracked. However, if the orthogonality is checked using

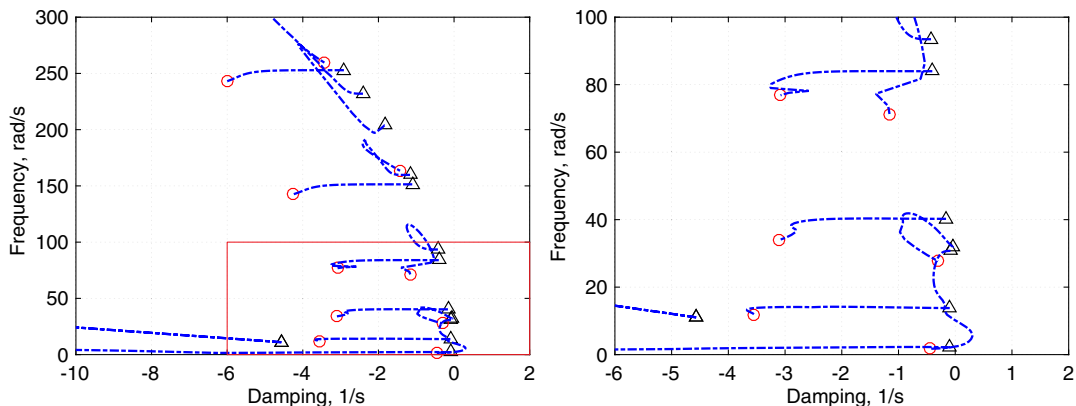


Fig. 12 Root locus plot of slender wing (triangle, 1 m/s; circle, 35 m/s).

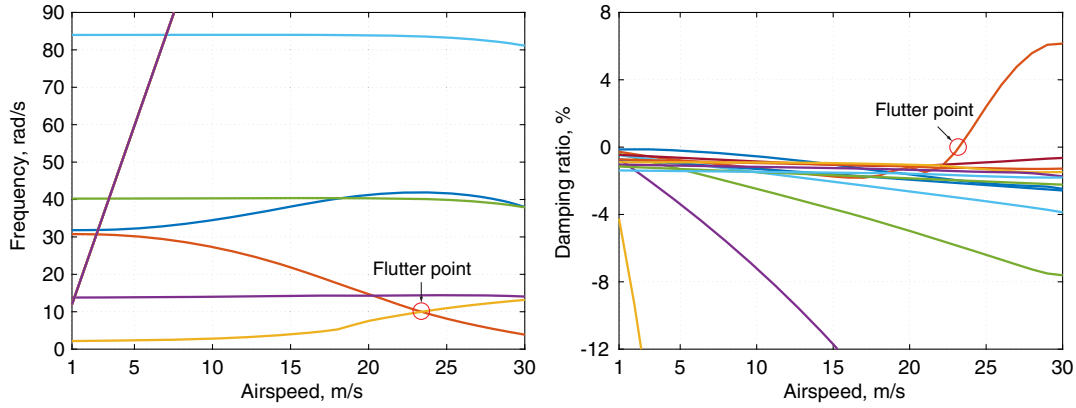


Fig. 13 Aeroelastic mode frequency (left) and damping ratio (right) vs airspeed around flutter point.

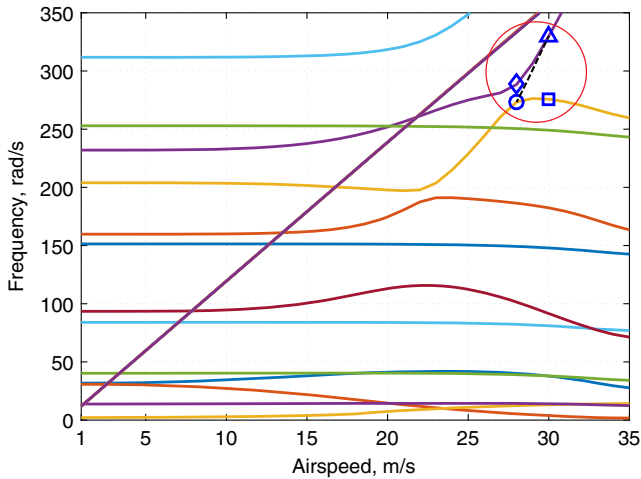


Fig. 14 Aeroelastic mode frequency vs airspeed.

both left and right eigenvectors, the orthogonality coefficient matrix becomes diagonally dominant, as shown in Fig. 16, indicating that every mode can be tracked correctly. These results verify the effectiveness and robustness of the mode tracking method based on left and right eigenvectors in the stability analysis of a nonlinear aeroelastic system.

A further study is carried out to more closely investigate the modes highlighted by the circle in Fig. 14. The mode tracking algorithm has identified them individually, with a mode coalescence and separation happening between 28 and 29 m/s. By reviewing the trend of eigenvalues, it is “possible” that the two modes may cross as indicated by the dashed line. From intuition, one would not expect a mode’s frequency to vary from 200 rad/s to more than 350 rad/s

within a small velocity range. The current mode tracking algorithm can show the correlation between the two modes around that region. In doing so, the speed increment is increased to 2 m/s (between 28 and 30 m/s), and the orthogonality check is performed on modes 10 and 11. The orthogonality coefficient matrix is shown in Fig. 17. The mode marked with the circle in Fig. 14 has the best correlation with the mode marked with the square, even with a larger velocity increment. This study verifies that the mode tracking result shown in Fig. 14, that is, the dashed path, cannot be an aeroelastic mode.

From the aeroelastic stability analysis with the mode tracking, it can be concluded that the mode tracking method based on left and right eigenvectors is feasible for use on geometrically nonlinear aeroelastic systems.

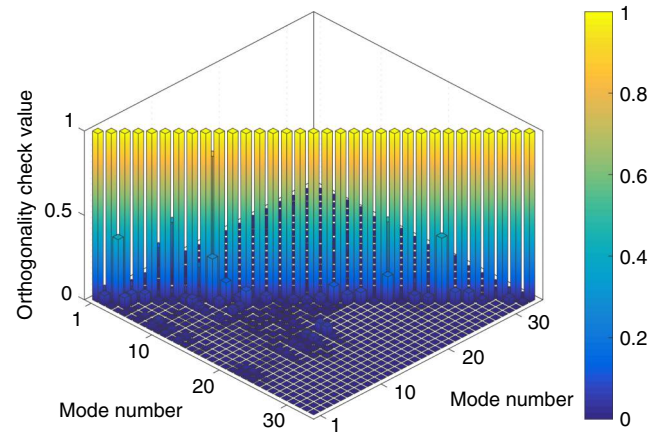


Fig. 16 Orthogonality coefficient matrix using current orthogonality check method (22 and 23 m/s).

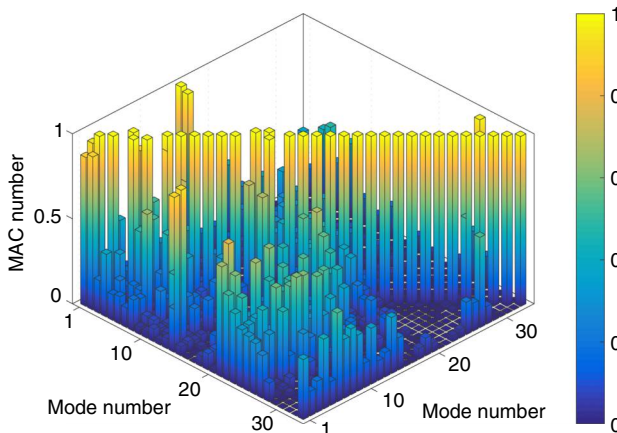


Fig. 15 Orthogonality coefficient matrix using MAC method (22 and 23 m/s).

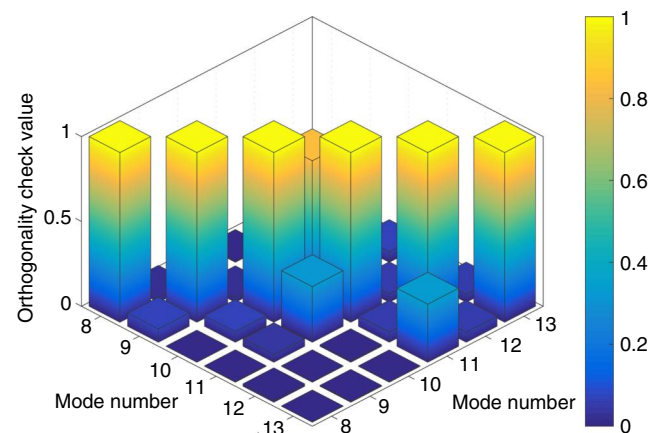


Fig. 17 Orthogonality coefficient matrix using current orthogonality check method (28 and 30 m/s).

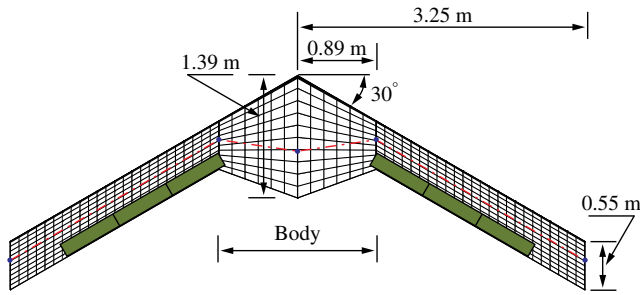


Fig. 18 Geometry of blended-wing-body configuration.

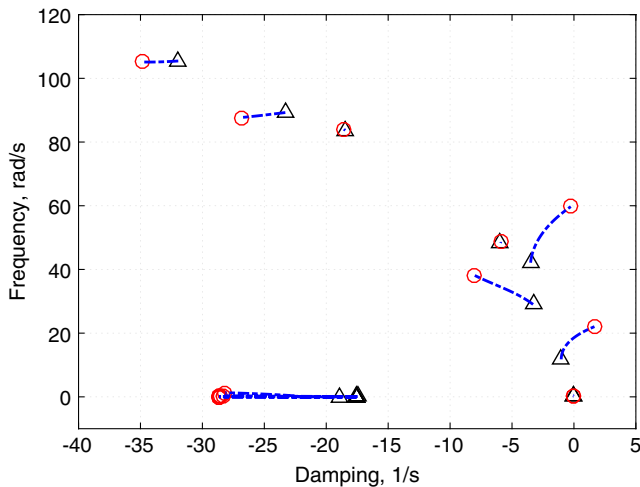


Fig. 19 Root locus of blended-wing-body configuration (triangle, 80 m/s; circle, 130 m/s).

D. Aircraft with Coupled Aeroelastic and Flight Dynamic Modes

A similar study is further performed on a blended-wing-body aircraft configuration, illustrated in Fig. 18 with more properties found in Su and Cesnik [25]. Both the body and the wings are modeled as strain-based beams coupled with finite-state unsteady aerodynamics. This model incorporates 6 beam elements in the body and 12 beam elements on each wing. For trim and maneuver purposes, elevons are defined on inner nine elements of the wing members. Note that the wings of this configuration are so flexible that their elastic modes are coupled with the rigid-body modes of the whole vehicle [25], resulting in a dynamic instability known as body-freedom flutter. In addition, the aeroelastic system matrix A has a dimension of 433 for the whole free-flight aircraft. Therefore, the mode tracking algorithm needs to recognize and track both elastic and rigid body modes correctly.

With the large dimension of the system matrix in this case and the interaction between aerodynamic modes and elastic/flight dynamic modes, several interfering eigenvalue pairs can be observed upon

solving the eigenvalue problem. Therefore, in this numerical case (also in the previous cases to some extent), a preliminary eigenvalue filtering is performed before the orthogonality check is applied. In addition, high-frequency modes that are not of interest are eliminated. Therefore, all eigenvalues with imaginary parts greater than 120 rad/s and real parts less than -40 rad/s are removed, where the cutoff values are chosen after an observation on the eigenvalues of the system. The root locus plot (Fig. 19) shows the variation tendency of the eigenvalues. One can clearly discern the aerodynamic-dominant modes (with large damping but small frequencies), rigid-body-dominant modes (with both small damping and frequencies), as well as the remaining elastic-dominant modes, even though all of them are coupled modes in reality. One mode (the first wing bending mode coupled with body pitching and plunging) crosses the imaginary axis around the velocity of 115 m/s, indicating the onset of aeroelastic instability. This stability boundary is close to the result reported by Su and Cesnik [25] ($V_f = 123$ m/s), where the difference is attributed to the different mesh and structural damping applied in the models. It can also be observed that some modes hardly change with the increase of airspeed in Fig. 19. All rigid-body modes are in a cluster around the origin point of the plot. To track their changes with the increase of velocity, the mode tracking method is applied with the orthogonality check using left and right eigenvectors, with the results shown in Fig. 20. As can be seen, all modes can be individually identified and separated from each other, even though the aerodynamic and rigid-body modes are numerically close together as shown in Fig. 19. From the V - g plot of Fig. 20, the flutter boundary can be identified, as there is only one damping ratio that crosses zero at 115 m/s.

IV. Conclusions

In this paper, a mode tracking method was developed for aeroelastic stability analysis, based on the orthogonality check of both the left and right eigenvectors of aeroelastic systems. The approach is adaptable to different aeroelastic formulations, as long as they can be transformed into a unified state-space representation. The method was demonstrated to be feasible for several frequently used unsteady aerodynamic theories and aeroelastic formulations. The detailed theoretical basis of the mode tracking technique using the left and right eigenvectors was highlighted in the paper, where two orthogonality checking matrices were used to track the aeroelastic modes. Numerical studies were conducted with different aeroelastic problems. The aeroelastic mode crossing phenomenon was first demonstrated with a 2-D airfoil. In the linear cantilever wing box and geometrically nonlinear cantilever wing cases, the proposed orthogonality check method was applied and compared with another model tracking method based on modal assurance criterion numbers of aeroelastic modes. The numerical results demonstrated that the newly developed method had a better capability in separating and tracking aeroelastic modes. The method was also more efficient as it allowed for larger velocity increment in the process of tracking, compared with the existing methods. Moreover, for the nonlinear blended-wing-body configuration with coupled aeroelasticity and flight dynamics, the results showed that the new method could

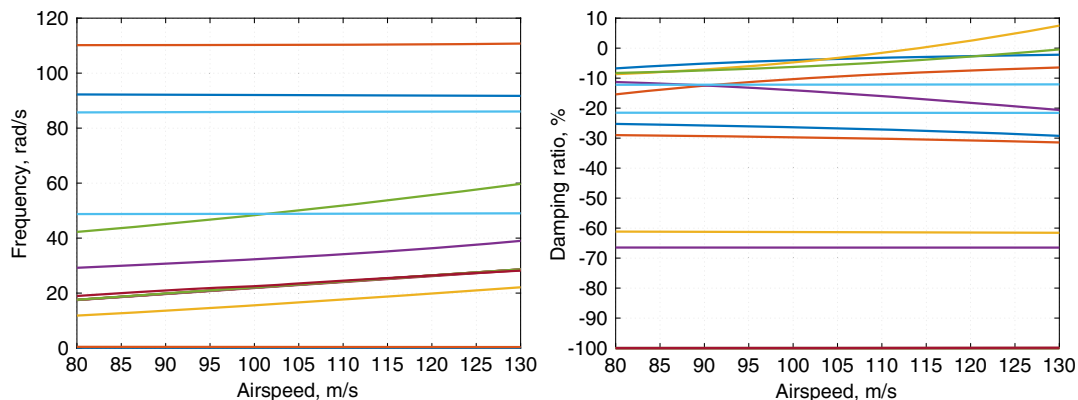


Fig. 20 Modal frequency (left) and damping (right) vs airspeed of blended-wing-body configuration.

successfully separate different types of modes with elastic-, aerodynamic-, or rigid-body dominance, respectively. It was also able to track the variation of rigid-body-dominant modes whose frequencies were close to zero. Through these numerical studies, advantages and effectiveness of the new mode tracking method using both the left and right eigenvectors have been demonstrated.

Acknowledgments

This work was partially supported by the China Scholarship Council (201606090064) and the Scientific Research Innovation Program of Jiangsu Province College Postgraduates (KYLX15_0092) of China. The authors would also like to acknowledge the University of Alabama for the support to this work.

References

- [1] Fung, Y. C., *An Introduction to the Theory of Aeroelasticity*, Dover Publ., New York, 1993, pp. 377–379.
- [2] Eldred, M. S., Venkayya, V. B., and Anderson, W. J., “New Mode Tracking Methods in Aeroelastic Analysis,” *AIAA Journal*, Vol. 33, No. 7, 1995, pp. 1292–1299. doi:10.2514/3.12552
- [3] Desmarais, R. N., and Bennett, R. M., “An Automated Procedure for Computing Flutter Eigenvalues,” *Journal of Aircraft*, Vol. 11, No. 2, 1974, pp. 75–80. doi:10.2514/3.60326
- [4] Van Zyl, L. H., “Use of Eigenvectors in the Solution of the Flutter Equation,” *Journal of Aircraft*, Vol. 30, No. 4, 1993, pp. 553–554. doi:10.2514/3.46380
- [5] Gibson, W. C., “ASTROS-ID: Software for System Identification Using Mathematical Programming,” CSA Engineering Inc. TR ADA260867, Palo Alto, CA, 1992.
- [6] Chen, P.-C., “Damping Perturbation Method for Flutter Solution: The g-Method,” *AIAA Journal*, Vol. 38, No. 9, 2000, pp. 1519–1524. doi:10.2514/2.1171
- [7] Huang, R., Qian, W. M., Zhao, Y. H., and Hu, H. Y., “Flutter Analysis: Using Piecewise Quadratic Interpolation with Mode Tracking and Wind-Tunnel Tests,” *Journal of Aircraft*, Vol. 47, No. 4, 2010, pp. 1447–1451. doi:10.2514/1.47687
- [8] Eller, D., “Flutter Equation as a Piecewise Quadratic Eigenvalue Problem,” *Journal of Aircraft*, Vol. 46, No. 3, 2009, pp. 1068–1070. doi:10.2514/1.40653
- [9] Mogenier, G., Baranger, T., Ferraris, G., Dufour, R., and Durantay, L., “A Criterion for Mode Shape Tracking: Application to Campbell Diagrams,” *Journal of Vibration and Control*, Vol. 20, No. 2, 2012, pp. 179–190. doi:10.1177/1077546312463714
- [10] *MSC Nastran 2018: Rotordynamics User's Guide*, MSC Software, Los Angeles, 2017, pp. 131–133.
- [11] Jones, R. T., “The Unsteady Lift of a Wing of Finite Aspect Ratio,” NACA TR-681, Washington, D.C., 1940.
- [12] Peters, D. A., and Johnson, M. J., “Finite-State Airloads for Deformable Airfoils on Fixed and Rotating Wings,” *Symposium on Aeroelasticity and Fluid/Structure Interaction, ASME Winter Annual Meeting*, Vol. AD-44, edited by P. P. Friedmann, and J. C. I. Chang, American Soc. of Mechanical Engineers, New York, 1994, pp. 1–28.
- [13] Peters, D. A., Karunamoorthy, S., and Cao, W.-M., “Finite State Induced Flow Models Part I: Two-Dimensional Thin Airfoil,” *Journal of Aircraft*, Vol. 32, No. 2, 1995, pp. 313–322. doi:10.2514/3.46718
- [14] Peters, D. A., and He, C.-J., “Finite State Induced Flow Models Part II: Three-Dimensional Rotor Disk,” *Journal of Aircraft*, Vol. 32, No. 2, 1995, pp. 323–333. doi:10.2514/3.46719
- [15] Eversman, W., and Tewari, A., “Consistent Rational-Function Approximation for Unsteady Aerodynamics,” *Journal of Aircraft*, Vol. 28, No. 9, 1991, pp. 545–552. doi:10.2514/3.46062
- [16] Wright, J. R., and Cooper, J. E., *Introduction to Aircraft Aeroelasticity and Loads*, 2nd ed., Wiley, West Sussex, U.K., 2014, pp. 450–453.
- [17] Roger, K. L., “Airplane Math Modeling Methods for Active Control Design,” *Structural Aspects of Active Controls, AGARD Conference Proceedings*, NATO Advisory Group for Aerospace Research and Development AGARD-CP-228, 1977, pp. 4/1–4/11.
- [18] Karpel, M., “Design for Active and Passive Flutter Suppression and Gust Alleviation,” NASA CR-3482, 1981.
- [19] Heimbaugh, R. M., “Flight Controls Structural Dynamics IRAD,” McDonnell-Douglas Company TR MDC-J2303, 1983.
- [20] Dykman, J. R., and Rodden, W. P., “An Application of the P-Transform Method for Transient Maneuvering Analysis,” *International Forum on Aeroelasticity and Structural Dynamics 1999*, edited by W. Whitlow, Jr., and E. N. Todd, NASA Langley Research Center, Hampton, VA, 1999, pp. 425–432.
- [21] Pitt, D., and Goodman, C., “FAMUSS - A New Aeroservoelastic Modeling Tool,” *33rd AIAA/ASME/ASCE/AHS/ASC Structures, Structural Dynamics, and Materials Conference*, AIAA Paper 1992-2395, 1992.
- [22] Baker, M. L., Goggin, P. J., and Winther, B. A., “Aeroservoelastic Modeling, Analysis, and Design Techniques for Transport Aircraft,” Defense Technical Information Center TR ADP010476, Fort Belvoir, VA, 2000.
- [23] Winther, B. A., Goggin, P. J., and Dykman, J. R., “Reduced-Order Dynamic Aeroelastic Model Development and Integration with Nonlinear Simulation,” *Journal of Aircraft*, Vol. 37, No. 5, 2000, pp. 833–839. doi:10.2514/2.2677
- [24] Palacios, R., Murua, J., and Cook, R., “Structural and Aerodynamic Models in Nonlinear Flight Dynamics of Very Flexible Aircraft,” *AIAA Journal*, Vol. 48, No. 11, 2010, pp. 2648–2659. doi:10.2514/1.J050513
- [25] Su, W., and Cesnik, C. E. S., “Nonlinear Aeroelasticity of a Very Flexible Blended-Wing-Body Aircraft,” *Journal of Aircraft*, Vol. 47, No. 5, 2010, pp. 1539–1553. doi:10.2514/1.47317
- [26] Rudisill, C. S., and Bhatia, K. G., “Optimization of Complex Structures to Satisfy Flutter Requirements,” *AIAA Journal*, Vol. 9, No. 8, 1971, pp. 1487–1491. doi:10.2514/3.6389
- [27] McIntosh, S. C., and Ashley, H., “On the Optimization of Discrete Structures with Aeroelastic Constraints,” *Computers & Structures*, Vol. 8, Nos. 3–4, 1978, pp. 411–419. doi:10.1016/0045-7949(78)90186-4
- [28] Hajela, P., “A Root Locus-Based Flutter Synthesis Procedure,” *Journal of Aircraft*, Vol. 20, No. 12, 1983, pp. 1021–1027. doi:10.2514/3.48206
- [29] Striz, A. G., and Venkayya, V. B., “Influence of Structural and Aerodynamic Modeling on Flutter Analysis,” *Journal of Aircraft*, Vol. 31, No. 5, 1994, pp. 1205–1211. doi:10.2514/3.46631
- [30] Jiang, L., Hang, X., and Fei, Q., “Mode Tracking Technique in Flutter Analysis Based on the Method of Orthogonality Check,” *Journal of Vibration and Shock*, Vol. 36, No. 19, 2017, pp. 84–89 (in Chinese). doi:10.13465/j.cnki.jvs.2017.19.013
- [31] Su, W., and Cesnik, C. E. S., “Strain-Based Geometrically Nonlinear Beam Formulation for Modeling Very Flexible Aircraft,” *International Journal of Solids and Structures*, Vol. 48, Nos. 16–17, 2011, pp. 2349–2360. doi:10.1016/j.ijsolstr.2011.04.012

D. Harursampath
Associate Editor